frontiers in Materials

ORIGINAL RESEARCH
published: 02 December 2021
doi: 10.3389/fmats.2021.717185

Suppression of the Cycloidal Spin Arrangement in $BiFeO_3$ Caused by the Mechanically Induced Structural Distortion and Its Effect on Magnetism

*Klebson Lucenildo Da Silva[1,2,3], Rafael Santiago Trautwein[1], Rodolfo Bezerra Da Silva[4], Martin Fabián[3], Erik Čižmár[5], Mariia Holub[5], Olha Skurikhina[3], Marta Harničárová[6,7], Vladimír Girman[5], Dirk Menzel[8], Klaus Dieter Becker[9], Horst Hahn[2] and Vladimír Šepelák[2,7]**

[1]Department of Physics, State University of Maringá, Maringá, Brazil, [2]Institute of Nanotechnology, Karlsruhe Institute of Technology, Eggenstein-Leopoldshafen, Germany, [3]Institute of Geotechnics, Slovak Academy of Sciences, Košice, Slovakia, [4]Department of Physics, Federal University of Rio Grande do Norte, Natal, Brazil, [5]Institute of Physics, Faculty of Science, P. J. Šafárik University, Košice, Slovakia, [6]Faculty of Engineering, Slovak University of Agriculture, Nitra, Slovakia, [7]Faculty of Technology, College of Technology and Business in České Budějovice, České Budějovice, Czech Republic, [8]Institute of Condensed Matter Physics, Braunschweig University of Technology, Braunschweig, Germany, [9]Institute of Physical and Theoretical Chemistry, Braunschweig University of Technology, Braunschweig, Germany

OPEN ACCESS

Edited by:
Faiz Pourarian, Carnegie Mellon University, United States

Reviewed by:
Doru Lupascu, University of Duisburg-Essen, Germany
Shengqiang Zhou, Helmholtz-Zentrum Dresden-Rossendorf, Germany
Shifeng Zhao, Inner Mongolia University, China

***Correspondence:**
Vladimír Šepelák
vladimir.sepelak@kit.edu

Specialty section:
This article was submitted to Thin Solid Films, a section of the journal Frontiers in Materials

Received: *30 May 2021*
Accepted: *10 November 2021*
Published: *02 December 2021*

Citation:
Da Silva KL, Trautwein RS, Da Silva RB, Fabián M, Čižmár E, Holub M, Skurikhina O, Harničárová M, Girman V, Menzel D, Becker KD, Hahn H and Šepelák V (2021) Suppression of the Cycloidal Spin Arrangement in $BiFeO_3$ Caused by the Mechanically Induced Structural Distortion and Its Effect on Magnetism. Front. Mater. 8:717185. doi: 10.3389/fmats.2021.717185

Bismuth ferrite ($BiFeO_3$) particles are prepared by a combined mechanochemical–thermal processing of a Bi_2O_3 + α-Fe_2O_3 mixture. Structural, magnetic, hyperfine, morphological and chemical properties of the as-prepared $BiFeO_3$ are studied using X-ray diffraction (Rietveld refinement), ^{57}Fe Mössbauer spectroscopy, SQUID magnetometry, electron microscopy and energy dispersive X-ray spectroscopy. It is revealed that the structure of the ferrite exhibits the long-range distortion (significantly tilted FeO_6 octahedra) and the short-range disorder (deformed FeO_6 octahedra). Consequently, these structural features result in the suppression of a space modulated cycloidal spin arrangement in the material. The latter manifests itself by the appearance of only single spectral component in the ^{57}Fe Mössbauer spectrum of $BiFeO_3$. The macroscopic magnetic behavior of the material is interpreted as a superposition of ferromagnetic and antiferromagnetic contributions with a large coercive field and remanent magnetization. Taking into account the average particle size of the as-prepared $BiFeO_3$ particles (~98 nm), exceeding the typical period length of cycloid (~62 nm), both the suppression of the spiral spin structure in the material and its partly ferromagnetic behavior are attributed to the crystal lattice distortion caused by mechanical stress during the preparation procedure.

Keywords: multiferroic, bismuth ferrite, cycloidal spin arrangement, mechanochemistry, Mössbauer spectroscopy

INTRODUCTION

Multiferroics have been the focus of numerous investigations because of their fascinating properties and potential applications. In particular, $BiFeO_3$ has attracted considerable attention due to its unique multiple functionalities (Castillo et al., 2013). It exhibits a strong coupling of electric, magnetic, and structural order parameters, giving rise to simultaneous ferroelectricity, antiferromagnetic G-type order at reasonable high temperatures, and ferroelasticity (Park et al., 2007; Da Silva et al., 2011; Bai et al., 2005). $BiFeO_3$ possesses a rhombohedrally distorted perovskite

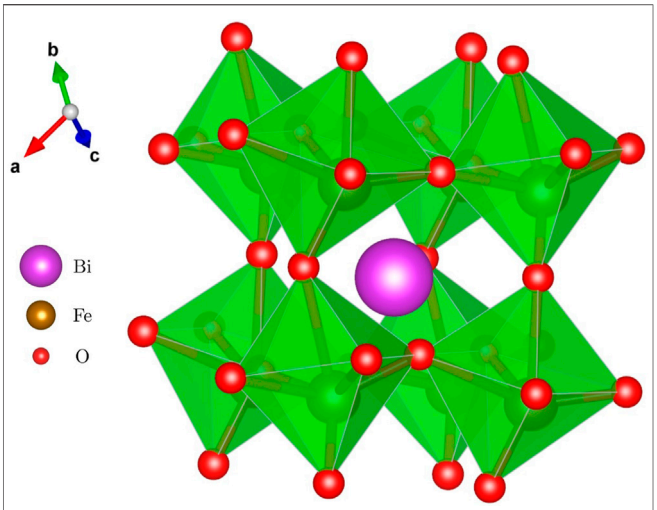

FIGURE 1 | Crystal structure of $BiFeO_3$ (space group *R3c*, No. 161) consists of Fe^{3+} cations octahedrally coordinated by oxygen ions. Bi^{3+} cations are excentrically located in the cavities formed by FeO_6 octahedra.

structure (space group *R3c*) with Bi^{3+} and Fe^{3+} cations displaced along the hexagonal [001]-axis (**Figure 1**). The material exhibits ferroelectric Curie temperature of about 1100 K. Magnetic moments of Fe^{3+} cations show a canted antiferromagnetic G-type ordering, which is a space long-wave modulated below the Néel temperature of 640 K (Yang et al., 2009; Fischer et al., 1980; Landers et al., 2014). The spin ordering manifests itself as an incommensurate cycloidal structure with a typical wavelength (λ) of about 62 nm along the hexagonal [001]-axis. Thus, the antiferromagnetic vector is locked within the cycloid, averaged to zero over λ (Bai et al., 2005).

It is known that the particle size reduction of $BiFeO_3$ below the typical period length of ~62 nm can lead to the suppression of its spiral spin structure, resulting in the ferromagnetic behavior of the nanomaterial (Mazumder et al., 2007; Park et al., 2007; Zhong et al., 2010; Castillo et al., 2013; Huang et al., 2013; Landers et al., 2014; Li et al., 2019). Additionally, the destruction of the cycloidal spin arrangement in $BiFeO_3$ can be induced by the crystal lattice distortion provoked by atom doping (Widatallah et al., 2014; Mao et al., 2016; Ting et al., 2017; Godara et al., 2018; Wang et al., 2018; Wang and Wang, 2018; Sharma et al., 2019; Xian et al., 2019; Dubey et al., 2020; Fertman et al., 2020; Sánchez-De Jesús et al., 2020). The present work gives evidence of the fact that the suppression of the cycloidal spin configuration in $BiFeO_3$ with the average particle size exceeding λ can also by caused by the mechanically induced crystal lattice distortion. Note that the alteration in the spin cycloid evoked by the lattice distortion and strain has also been reported for multiferroic $BiFeO_3$ films (Xing et al., 2014; Yang et al., 2015).

The performance of multiferroics is closely related to the ways in which they are processed. The conventional solid-state synthesis of $BiFeO_3$ requires prolonged and sometimes repeated treatment of its precursors at considerably high calcination temperatures (Kothari et al., 2008), causing the loss of bismuth due to its high volatility. The latter results in the formation of multiphase products and, consequently, in the degradation of microstructural and functional properties of the multiferroic material (Ghosh et al., 2005; Kong et al., 2008). Various wet chemistry-based routes have also been developed to synthesize nanosized multiferroic powders (Mazumder et al., 2007; Selbach et al., 2007; Fruth et al., 2007). Among the many processing techniques, the nonconventional mechanochemical route has been recognized as a powerful method for the production of multiferroics (Da Silva et al., 2011; Šepelák et al., 2013; Avvakumov et al., 2001). The continued development of mechanochemistry, as a field of chemical sciences dealing with transformations of solids induced by mechanical energy (Michalchuk et al., 2021), promises to revolutionize the chemical industry (James et al., 2012), providing one-step synthetic routes to various metastable and nonequilibrium materials at ambient temperature directly from their precursors, mostly in the form of nanosized powders, without the need for calcination at intermediate temperatures, thus making the process very simple and effective (Šepelák et al., 2013).

In the present work, $BiFeO_3$ particles with the size exceeding the typical period length of ~62 nm are prepared via mechanochemical processing (high-energy milling) of a Bi_2O_3 + α-Fe_2O_3 mixture followed by its relatively short (5 min) thermal treatment at 973 K. The as-prepared material is characterized by means of Rietveld refinement of X-ray diffraction (XRD) data, ^{57}Fe Mössbauer spectroscopy, electron microscopy, SQUID magnetometry, and energy dispersive X-ray (EDX) spectroscopy. It is demonstrated that the ferrite possesses the destructed cycloidal spin arrangement due to the structural distortion caused by mechanical stress induced by high-energy milling during the preparation procedure. Consequently, unusual ferromagnetic behavior with a high coercive field and remanent magnetization in the as-prepared $BiFeO_3$ is reported.

MATERIALS AND METHODS

$BiFeO_3$ subjected to the present investigations was prepared from the stoichiometric mixture of Bi_2O_3 (Alfa Aesar, 99.999%) and α-Fe_2O_3 (Alfa Aesar, 99.998%) precursors with the initial average particle sizes of 0.5 and 0.7 μm, respectively. At first, the mixture was milled in a high-energy planetary mill Pulverisette 6 (Fritsch, Germany) for 12 h. The milling chamber (250 cm^3 in volume) and 22 balls (10 mm in diameter), both made of tungsten carbide, were used. The ball-to-powder weight ratio was 22:1. Milling experiment was performed in air at 600 rpm. The second step of the mechanochemical–thermal preparation route included the thermal processing of the powdered sample at 973 K for 5 min.

Additionally, microcrystalline $BiFeO_3$, which served as a *reference sample* in this study, was prepared from equimolar amounts of reagent-grade oxides (Bi_2O_3 and α-Fe_2O_3) by the conventional solid-state (ceramic) route. Powdered reactants were, at first, homogenized under ethanol in an agate mortar and then pressed into tablets (20 mm in diameter, 4 mm thick) under uniaxial pressure of 30 MPa in a steel mould in order to obtain a high degree of compaction. The reaction tablets were

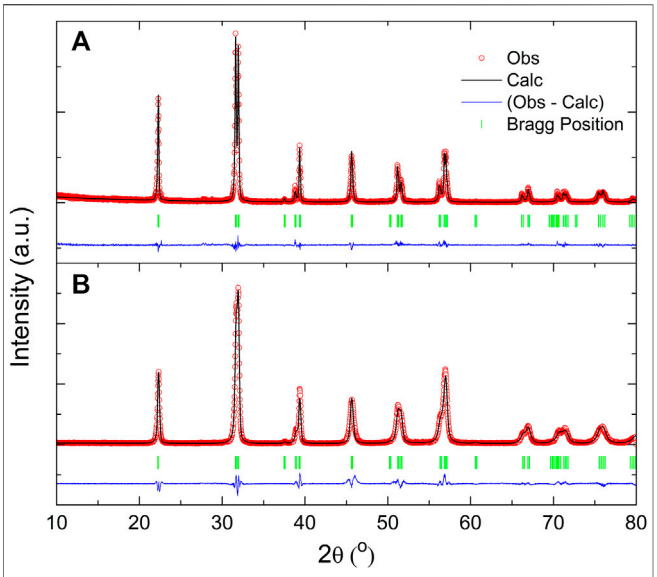

FIGURE 2 | The refined XRD patterns of **(A)** $BiFeO_3$ synthesized by the ceramic method and **(B)** $BiFeO_3$ prepared by the combined mechanochemical–thermal route.

prefired twice at 1300 K for 24 h, reground, pressed, and finally sintered at 1400 K for 24 h. The single-phase nature of the microcrystalline $BiFeO_3$ (with the average crystallite size of 0.7 μm) was confirmed by X-ray diffraction and ^{57}Fe Mössbauer spectroscopy.

The XRD patterns of the samples were measured using a PW 1820 X-ray diffractometer (Philips, Netherlands), operating in Bragg configuration and using Cu Kα radiation. The XRD scans were collected from 10° to 80° (2θ), using a step of 0.02° and a data collection time of 5 s. Rietveld refinements of XRD data were performed using the *FullProf Suite* software (Rodríguez-Carvajal, 2019). Rietveld analyses of XRD data provided the crystal structure parameters (*a*, *b*, *c*, *V*) and the exact atomic coordinates (*x*, *y*, *z*) of the constituent atoms in the materials. The bond angles and the interatomic distances were calculated on the basis of the derived coordinates of the corresponding atoms using the *Vesta* program (Momma and Izumi, 2011). The Inorganic Crystal Structure Database (ICSD) was utilized for phase identification. The 3-dimmensional structure of the as-prepared material (**Figure 1**) was visualized using the *Vesta* program (Momma and Izumi, 2011).

^{57}Fe Mössbauer spectra were taken at 293 K in transmission geometry using a ^{57}Co/Rh γ-ray source (manufactured by Ritverc, Russia) with the activity of 50 mCi. The optimal amount of the powdered sample, calculated using Recoil software (Lagarec and Rancourt, 1998), was mixed with sucrose to assist in spreading the sample evenly across the sample holder with the diameter of 1 cm. To obtain the transmission spectra with a sufficiently good count statistics, the collection of the ^{57}Fe Mössbauer data took 48 h. Recoil spectral analysis software (Lagarec and Rancourt, 1998) was used for the quantitative evaluation of the Mössbauer spectra. The Voigt-based fitting method provided distributions of hyperfine parameters for multiple sites in a spectrum. A Lorentzian line half-width of 0.17 mm/s resulting from the fit of the spectrum of the reference microcrystalline $BiFeO_3$ was chosen for the fit of the spectrum of the as-prepared $BiFeO_3$. The derived isomer shifts (IS) are given relative to IS of α-Fe at room temperature.

TABLE 1 | Crystal structure parameters (*a*, *b*, *c*, *V*), atomic positions (*x*, *y*, *z*), and the tilting angle of FeO_6 octahedra derived from the Rietveld analysis of XRD data of the as-prepared $BiFeO_3$. R_p, R_{wp} and χ^2 are goodness parameters of the fit.

Formula		**$BiFeO_3$**	
Crystal system		rhombohedral	
Space group		*R3c*	
a, Å		5.5715(5)	
b, Å		5.5715(5)	
c, Å		13.8185(15)	
V, Å^3		371.49(6)	
Atomic positions	*x*	*y*	*z*
Bi (6*a*)	0.0000(0)	0.0000(0)	0.0000(0)
Fe (6*a*)	0.0000(0)	0.0000(0)	0.2719(4)
O (18*b*)	0.4485(21)	0.0294(23)	0.9521(5)
Fe—O—Fe bond angle		127.2°	
R_p, R_{wp}; χ^2		9.36%, 12.9%; 3.33	

The morphology of powders was studied using a combined field-emission (scanning) transmission electron microscope (S)TEM (JEOL JEM-2100F UHR) operated at 200 kV. The (S)TEM-bright field mode was used for imaging of powder particles. For (S)TEM analysis, the powdered samples were diluted in distilled water and ultrasonicated. A droplet of the water-diluted colloidal suspension was deposited on copper grid coated with lacey carbon film. The grids were dried in vacuum.

Magnetic measurements were performed at 300 and 5 K in external magnetic fields (H_{ext}) from 0 to ±5 T using a SQUID magnetometer (Quantum Design MPMS-5S). The powdered samples were filled in a small container made of polyvinyl chloride, whose diamagnetic moment was subtracted from the measured magnetization (*M*) values. At first, the M-H_{ext} measurement of the empty sample container was performed. Then the powdered $BiFeO_3$ sample was filled in the container and the magnetization data were collected. The net magnetization data of the ferrite were obtained as the difference of measured magnetization values of the filled container and the empty one.

RESULTS AND DISCUSSION

Figure 2 compares the XRD patterns of *the reference material* synthesized by the ceramic method and the material prepared by the combined mechanochemical–thermal route (further referred to as *the as-prepared material*). Rietveld analyses of the XRD data reveal that the patterns are well-fitted using a single rhombohedral phase (ICSD collection code 8823) with space group *R3c*. No spurious or minority phase has been observed. It clearly demonstrates that both the ceramic method and the combined mechanochemical–thermal route lead to the formation of the desired $BiFeO_3$ phase. The crystal structure parameters of the as-prepared phase, derived from the Rietveld

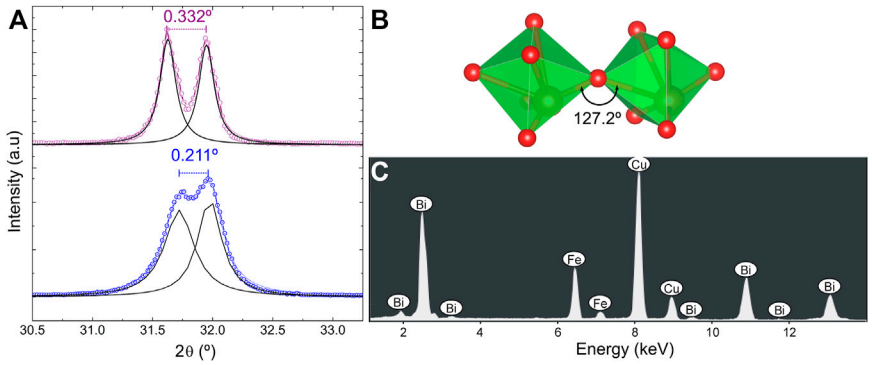

FIGURE 3 | (A) XRD peaks corresponding to the (110) **(right)** and (104) **(left)** crystallographic planes for $BiFeO_3$ samples prepared by the conventional ceramic method (purple pattern) and the combined mechanochemical–thermal route (blue pattern). **(B)** The neighboring FeO_6 octahedra in the crystal lattice of the as-prepared $BiFeO_3$ exhibit a relatively small tilting angle of about 127.2°. **(C)** EDX spectrum of the as-prepared $BiFeO_3$.

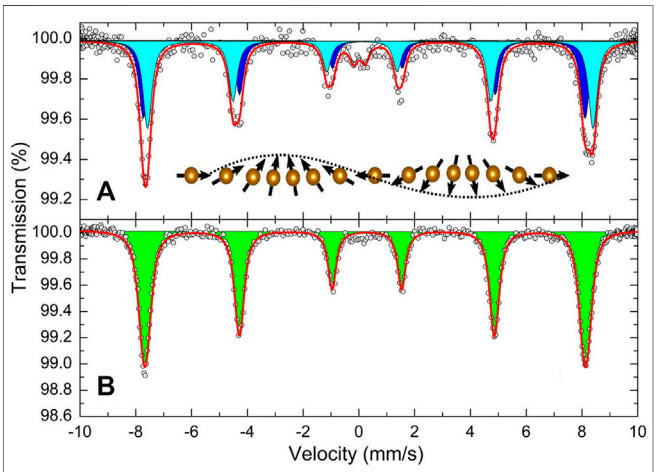

FIGURE 4 | Room-temperature ^{57}Fe Mössbauer spectra of **(A)** $BiFeO_3$ synthesized by the ceramic method and **(B)** $BiFeO_3$ prepared by the combined mechanochemical–thermal route. The inset schematically shows the cycloidal arrangement of spins in the reference $BiFeO_3$ synthesized by the ceramic method.

analysis, are listed in **Table 1**. An important observation is that the lattice parameters of the rhombohedral structure of the as-prepared ferrite ($a = b = 5.5715(5)$ Å, $c = 13.8185(15)$ Å) are smaller when compared with those of the reference $BiFeO_3$ sample ($a = b = 5.592$ Å, $c = 13.898$ Å) (Selbach et al., 2007; Godara et al., 2018; Wang et al., 2018; Xian et al., 2019; Sánchez-De Jesús et al., 2020).

The lattice shrinkage is clearly visible in **Figure 3A**, where XRD peaks corresponding to the (110) and (104) crystallographic planes are compared for $BiFeO_3$ samples prepared by the combined mechanochemical–thermal route (blue pattern) and conventional way (purple pattern). The corresponding angular differences between the two planes are 0.211° and 0.332° (2θ) for the as-prepared ferrite and the reference material, respectively. As a consequence of the lattice shrinkage, the neighboring FeO_6 octahedra in the crystal lattice of the as-prepared $BiFeO_3$ exhibit a relatively small tilting angle of 127.2° (**Figure 3B**). Note that the Fe—O—Fe bond angle in the lattice of the reference microcrystalline material is 150.9° (Sharma et al., 2019). The effect of such long-range crystal lattice distortion on magnetism of the as-prepared material is discussed below.

To exclude the presence of chemical elements originating from the abrasion of the milling tools (vial and balls made of WC) during the mechanochemical–thermal preparation route, we carried out the energy dispersive X-ray analysis of the as-prepared material. As can be seen in the representative EDX spectrum (**Figure 3C**), the only constituent chemical elements, Bi and Fe, were detected in the sample. Note that the spectral lines corresponding to Cu in the EDX spectrum originate from the copper-supported carbon grid.

^{57}Fe Mössbauer spectroscopy as a nuclear method is employed to investigate of the local coordination, the magnetic state, the spin arrangement and the charge states of iron ions in both the reference and as-prepared $BiFeO_3$ samples. **Figure 4** compares the room-temperature ^{57}Fe Mössbauer spectra of the as-prepared $BiFeO_3$ and its microcrystalline counterpart. The asymmetric spectrum of the reference sample (**Figure 4A**) is fitted by a superposition of two subspectra (sextets) reflecting the presence of the cycloidal arrangement of spins of Fe^{3+} cations (Landers et al., 2014). Note that within the cycloid, a part of spins is oriented antiparallelly to another part of spins, resulting in the zero antiferromagnetic vector (see inset of **Figure 4A**). The hyperfine parameters of ferric ions resulting from the least-squares fitting of the spectrum are presented in **Table 2**.

In contrast to the reference sample, ^{57}Fe Mössbauer spectrum of the as-prepared $BiFeO_3$ (**Figure 4B**) is symmetrical and consists of only one sextet assigned to the high-spin ferric cations in octahedral coordination of oxygen ions; see the corresponding hyperfine parameters listed in **Table 2** (Menil, 1985). It should be emphasized that the presence of only single spectral component in the Mössbauer spectrum is a clear evidence of the suppression of the cycloidal arrangement of spins in the as-prepared $BiFeO_3$.

TABLE 2 | Parameters obtained by fitting the room-temperature ^{57}Fe Mössbauer spectra of $BiFeO_3$ samples synthesized by two various routes. IS is the isomer shift; QS is the quadrupole splitting; σ is the Gaussian width of the spectral component; B_{hf} is the magnetic hyperfine field; *I* is the relative intensity of the spectral component.

Material	Spectral component	IS (mm/s)	QS (mm/s)	σ (mm/s)	B_{hf} (T)	*I* (%)
the references $BiFeO_3$	sextet (light blue)	0.370(10)	0.15(2)	0.31(3)	49.5(1)	50.2(62)
	sextet (dark blue)	0.358(11)	−0.06(2)	0.32(3)	49.1(1)	44.5(62)
	doublet[a]	0.129(65)	0.41(10)	0.07(3)	—	5.3(12)
the as-prepared $BiFeO_3$	sextet (green)	0.367(2)	−0.03(0)	0.76(3)	48.99(2)	100

[a]*The doublet spectral component corresponds to a small fraction (~5.3%) of fine $BiFeO_3$ particles exhibiting superparamagnetism at room temperature.*

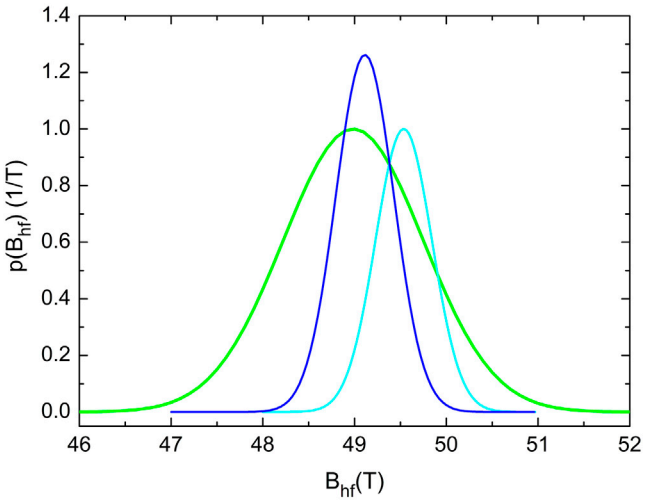

FIGURE 5 | HFDs derived from the ^{57}Fe Mössbauer spectra of the reference $BiFeO_3$ (dark and light blue lines) and the as-prepared $BiFeO_3$ (green line).

Another striking feature of the present Mössbauer data is the observed difference between the Gaussian widths (σ) of the sextets for the reference material and the as-prepared ferrite (see **Table 2**). **Figure 5** compares the hyperfine field distributions (HFDs) derived from the Mössbauer spectra of both materials. It should be emphasized that HFDs provide the most detailed information on the local magnetic fields acting on iron nuclei located on a particular lattice site. As can be seen, the iron nuclei in the reference $BiFeO_3$ experience the local fields from relatively narrow intervals (from about 48 to 50 T and from about 48.4 to 50.5 T). This is in contrast to the as-prepared material, where a broad HFD is observed ranging from about 47 to 51 T; see green line in **Figure 5**. This variation may be explained by the presence of a broad distribution of local environments around the Fe nuclei in the as-prepared material due to a strongly distorted geometry of FeO_6 octahedra. Similar findings have also been reported for other mechanochemically prepared oxides (Šepelák et al., 2006; Šepelák et al., 2007; Šepelák et al., 2009). Thus, in addition to the distorted mutual orientation of FeO_6 octahredra characterized by the tilting angle of about 127°, revealed by Rietveld method (see above), the present Mössbauer data provide clear evidence of the presence of strongly deformed structural FeO_6 units in the as-prepared material.

To determine the origin of the suppression of the cycloidal spin arrangement and to exclude its alteration due to the particle size effect (the presence of particles with the size below the typical period length of cycloid (~62 nm)), we found it necessary to perform (S)TEM investigations of the as-prepared material. The representative (S)TEM micrograph of the ferrite is shown in **Figure 6A**. The $BiFeO_3$ particles are found to be roughly spherical (closely to rectangular), and they tend to agglomerate. It has been revealed that the as-prepared material consists of particles mostly in the 60–130 nm size range; thus, the major part of particles is larger than the typical period length of cycloid. Note that a small part (~8% by volume) of the as-prepared $BiFeO_3$ particles is smaller than 62 nm. Taking into account the average particle size $D_a = 98 \pm 8$ nm of the ferrite (see **Figure 6B**) and the results of the present XRD and Mössbauer investigations presented above, we attribute the suppression of the spiral spin structure in the as-prepared material mainly to its long-range structural distortion (tilting of FeO_6 octahedra) and the short-range structural disorder (deformation of FeO_6 octahedra). Obviously, a small part of particles with the size below the typical period length of cycloid also partly contributes to the suppression of the spin cycloid in the as-prepared $BiFeO_3$.

SQUID measurements have revealed that magnetic behavior of the as-prepared $BiFeO_3$ is different from that of the reference microcrystalline $BiFeO_3$ prepared using the conventional ceramic method. The latter sample does not show the hysteresis behavior (see our previous work (Da Silva et al., 2011)), whereas the as-prepared material exhibits extraordinarily high values of coercive field (H_c ~ 0.71 T at 5 K, H_c ~ 1.1 T at 300 K) and remanent magnetization (M_r ~ 0.15 emu/g at 5 K, M_r ~ 0.13 emu/g at 300 K) (see **Table 3** and **Figure 7**). Note that values of these quantities for the as-prepared ferrite are significantly larger than those observed for the doped $BiFeO_3$ with the consequently "chemically" induced structural distortion (Mao et al., 2016; Wang et al., 2018; Sharma et al., 2019; Fertman et al., 2020).

The magnetization hysteresis loops of the material measured at 5 and 300 K, depicted in **Figure 7A**, can be interpreted as a superposition of ferromagnetic and antiferromagnetic contributions. The dominant contribution of ferromagnetism is here observed as a broad saturated hysteresis, which is superimposed by the linear (nonsaturated) minor part without hysteresis induced by the presence of a weak antiferromagnetism. The linear dependences $M(H_{ext}) = 0.068 \cdot H_{ext}$ and $M(H_{ext}) = 0.06854 \cdot H_{ext}$ were used to calculate the contribution of

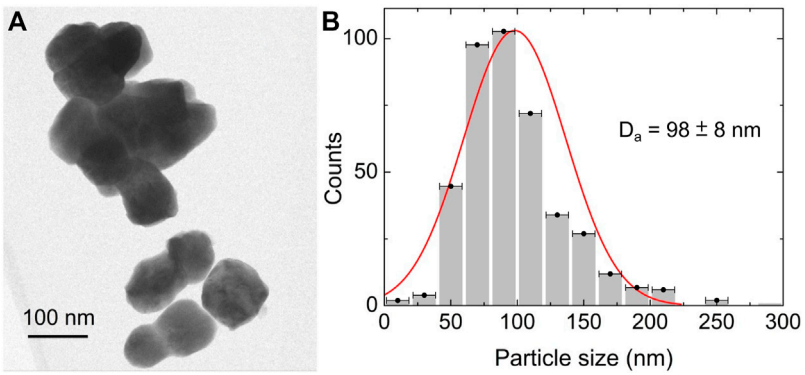

FIGURE 6 | (A) The (S)TEM image of $BiFeO_3$ prepared by the combined mechanochemical–thermal route. **(B)** The particle size distribution in the material results in the average particle size D_a = 98 ± 8 nm. The error bars showing the uncertainty in the particle size analysis are indicated.

TABLE 3 | Parameters of the ferromagnetic part of the magnetization hysteresis loops recorded at 5 and 300 K for the as-prepared $BiFeO_3$. H_c is the coercive field; M_r is the remanent magnetization; M_s is the saturation magnetization.

Temperature (K)	H_c (T)	M_r (emu/g)	M_s (emu/g)	M_r/M_s
5	0.7056	0.15	0.16	0.93
300	1.0592	0.13	0.14	0.92

antiferromagnetism at 5 and 300 K, respectively. The net magnetization data of the ferromagnetic contribution were obtained as the difference of the measured values of total magnetization and the calculated $M(H_{ext})$ values corresponding to the antiferromagnetic contribution. The ferromagnetic contribution of the as-prepared ferrite separated from the antiferromagnetic one is shown in **Figure 7B**.

It is worth to mention that the saturation magnetization (M_s) of the ferromagnetic contribution attains the values of about 0.16 and 0.14 emu/g at 5 and 300 K, respectively. These M_s values represent about 32 and 29% of the total magnetization (for H_{ex} = 5 T) of the as-prepared sample at 5 and 300 K, respectively. Taking into account the presence of the long-range and short-range structural distortions in the material, the ferromagnetic contribution can be interpreted as to arise from the destroyed

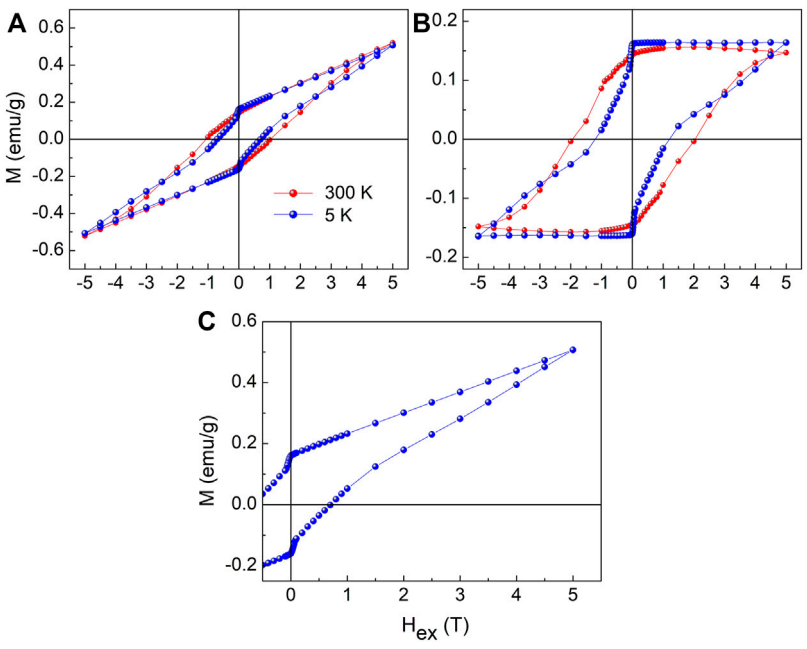

FIGURE 7 | (A) Magnetization hysteresis loops for the as-prepared $BiFeO_3$ measured at 5 K (blue line) and 300 K (red line). **(B)** The ferromagnetic components for the as-prepared $BiFeO_3$ extracted from its magnetization hysteresis loops measured at 5 K (blue line) and 300 K (red line). **(C)** The $M(H_{ext})$ curve measured at 5 K for the as-prepared $BiFeO_3$ in the field region of –0.5 T < H_{ext} < 5 T showing the wasp-waisted behavior.

cycloidal spin arrangement and the appearance of the Fe^{3+}—O^{-2}—Fe^{3+} exchange paths with deformed tilting angles of about 127°. These bond angles play a major role in controlling the magnetic exchange and orbital overlap between Fe^{3+}—O^{-2} ions. Additionally, the structural distortion can lead to the onset of the Dzyaloshinskii–Moriya (D–M) interaction (Sharma et al., 2019; Yang et al., 2012; Albrecht et al., 2010), which can play a significant role in enhancing the ferromagnetism in the as-prepared sample. It should be mentioned that the D–M interaction is the antisymmetric magnetic exchange coupling leading to the noncollinear (canted) spin states, which are located at the interface between the ferromagnetic and antiferromagnetic regions present in the as-prepared material. Note that the hysteresis loop recorded at 5 K exhibits a wasp-waisted behavior (Pinheiro et al., 2020) with an abrupt change in magnetization for a field close to zero, in both the descending and ascending curves (see **Figure 7C**). We attribute this phenomenon to the reorientation of canted spins, which are located at the interface between the ferromagnetic and antiferromagnetic regions present in the as-prepared ferrite.

CONCLUSION

The combined mechanochemical–thermal treatment of the Bi_2O_3 and α-Fe_2O_3 precursors leads to the formation of the rhombohedral $BiFeO_3$ with the lattice parameters ($a = b$ = 5.5715(5) Å, c = 13.8185(15) Å) that are smaller when compared with those of the reference $BiFeO_3$ synthesized by the conventional route ($a = b$ = 5.592 Å, c = 13.898 Å). At the long-range scale, neighboring FeO_6 octahedra in the crystal lattice of the as-prepared $BiFeO_3$ exhibit a relatively small tilting angle of 127.2° in comparison with the Fe—O—Fe bond angle of 150.9° characteristic of the reference material. ^{57}Fe Mössbauer spectroscopy reveals that, at the short-range scale, the structure of the material is characterized by a broad distribution of local environments around the Fe nuclei due to a strongly distorted geometry of FeO_6 octahedra. The presence of only single spectral component in the ^{57}Fe Mössbauer spectrum of the as-prepared ferrite is a clear evidence of the suppression of the cycloidal spin arrangement in its structure. It is revealed that the material consists of particles mostly in the 60–130 nm size range, resulting in the average particle size of 98 ± 8 nm. Considering this value, which exceeds the typical period length of cycloid (~62 nm), it is stated that the suppression of the cycloidal spin arrangement in the as-prepared $BiFeO_3$ is mainly caused by the long- and short-range crystal lattice distortions. The minor contribution to the suppression of the spin cycloid is represented by the particle size effect. The macroscopic magnetic properties of the material are interpreted as a superposition of antiferromagnetic and ferromagnetic contributions. The latter is characterized by extraordinarily high values of coercive field (H_c ~ 0.71 T at 5 K, H_c ~ 1.1 T at 300 K) and remanent magnetization (M_r ~ 0.15 emu/g at 5 K, M_r ~ 0.13 emu/g at 300 K). A partly ferromagnetic behavior of the ferrite is attributed to the suppressed cycloidal spin arrangement and the appearance of the Fe^{3+}—O^{-2}—Fe^{3+} exchange paths with deformed tilting angles. At the interface between the ferromagnetic and antiferromagnetic regions, the D–M interaction leads to the canted spin states. An abrupt change in magnetization of $BiFeO_3$ for a field close to zero, in both the descending and ascending $M(H_{ex})$ curves, is attributed to the reorientation of canted spins.

DATA AVAILABILITY STATEMENT

The raw data supporting the conclusion of this article will be made available by the authors, without undue reservation.

AUTHOR CONTRIBUTIONS

VŠ: Principal Investigator of the project; Conceptualization; Supervision; Mössbauer investigations; Data interpretation; Resources; Writing—original draft. KD: Conceptualization; Supervision; XRD investigations; Data interpretation; Formal analysis; Writing—original draft. RT: Visualization; Investigation. RD: Methodology, Data interpretation. MF: Software, Formal analysis. EČ, MH, and DM: SQUID investigations; Data interpretation. OS and MH: Sample preparation; Formal analysis. VG: S(TEM) investigations. KB and HH: Conceptualization; Supervision.

FUNDING

The present work is supported by the DFG (project SE 1407/4-2), the CAPES, and the APVV (project 19-0526). KD thanks the Karlsruhe Institute of Technology (KIT) and the SAIA for supporting his research work at KIT and the Slovak Academy of Sciences, respectively. This work benefited from networking activities carried out within the EU funded COST Action CA18112 "Mechanochemistry for Sustainable Industry" and represents a contribution to it. We acknowledge support by the KIT-Publication Fund.

REFERENCES

Albrecht, D., Lisenkov, S., Ren, W., Rahmedov, D., Kornev, I. A., and Bellaiche, L. (2010). Ferromagnetism in Multiferroic $BiFeO_3$ Films: A First-Principles-Based Study. *Phys. Rev. B.* 81 (14), 140401. doi:10.1103/PhysRevB.81.140401

Avvakumov, G. V., Senna, M., and Kosova, N. V. (2001). *Soft Mechanochemical Synthesis: A Basis for New Chemical Technologies*. Boston: Kluwer Academic Publishers.

Bai, F., Wang, J., Wuttig, M., Li, J., Wang, N., Pyatakov, A. P., et al. (2005). Destruction of Spin Cycloid in (111)c-Oriented BiFeO3 Thin Films by Epitiaxial Constraint: Enhanced Polarization and Release of Latent Magnetization. *Appl. Phys. Lett.* 86 (3), 032511. doi:10.1063/1.1851612

Castillo, M. E., Shvartsman, V. V., Gobeljic, D., Gao, Y., Landers, J., Wende, H., et al. (2013). Effect of Particle Size on Ferroelectric and Magnetic Properties of $BiFeO_3$ Nanopowders. *Nanotechnology* 24 (35), 355701. doi:10.1088/0957-4484/24/35/355701

Da Silva, K. L., Menzel, D., Feldhoff, A., Kübel, C., Bruns, M., Paesano, A., et al. (2011). Mechanosynthesized $BiFeO_3$ Nanoparticles with Highly Reactive Surface and Enhanced Magnetization. *J. Phys. Chem. C.* 115 (15), 7209–7217. doi:10.1021/jp110128t

Dubey, A., Escobar Castillo, M., Landers, J., Salamon, S., Wende, H., Hagemann, U., et al. (2020). Effect of Mn and Ba Codoping on a Magnetic Spin Cycloid of Multiferroic Bismuth Ferrite Nanoparticles. *J. Phys. Chem. C.* 124 (40), 22266–22277. doi:10.1021/acs.jpcc.0c05778

Fertman, E. L., Fedorchenko, A. V., Čižmár, E., Vorobiov, S., Feher, A., Radyush, Y. V., et al. (2020). Magnetic Diagram of the High-Pressure Stabilized Multiferroic Perovskites of the $BiFe_{1-y}Sc_yO_3$ Series. *Crystals* 10 (10), 950. doi:10.3390/cryst10100950

Fischer, P., Polomska, M., Sosnowska, I., and Szymanski, M. (1980). Temperature Dependence of the Crystal and Magnetic Structures of $BiFeO_3$. *J. Phys. C: Solid State. Phys.* 13 (10), 1931–1940. doi:10.1088/0022-3719/13/10/012

Fruth, V., Tenea, E., Gartner, M., Anastasescu, M., Berger, D., Ramer, R., et al. (2007). Preparation of $BiFeO_3$ Films by Wet Chemical Method and Their Characterization. *J. Eur. Ceram. Soc.* 27 (2-3), 937–940. doi:10.1016/j.jeurceramsoc.2006.04.135

Ghosh, S., Dasgupta, S., Sen, A., and Maiti, H. S. (2005). Low Temperature Synthesis of Bismuth Ferrite Nanoparticles by a Ferrioxalate Precursor Method. *Mater. Res. Bull.* 40 (12), 2073–2079. doi:10.1016/j.materresbull.2005.07.017

Godara, P., Agarwal, A., Ahlawat, N., and Sanghi, S. (2018). Crystal Structure, Dielectric and Magnetic Properties of Gd Doped $BiFeO_3$ Multiferroics. *Physica B: Condensed Matter* 550, 414–419. doi:10.1016/j.physb.2018.08.045

Huang, F., Wang, Z., Lu, X., Zhang, J., Min, K., Lin, W., et al. (2013). Peculiar Magnetism of $BiFeO_3$ Nanoparticles with Size Approaching the Period of the Spiral Spin Structure. *Sci. Rep.* 3, 2907. doi:10.1038/srep02907

James, S. L., Adams, C. J., Bolm, C., Braga, D., Collier, P., Friščić, T., et al. (2012). Mechanochemistry: Opportunities for New and Cleaner Synthesis. *Chem. Soc. Rev.* 41 (1), 413–447. doi:10.1039/c1cs15171a

Kong, L. B., Zhang, T. S., Ma, J., and Boey, F. (2008). Progress in Synthesis of Ferroelectric Ceramic Materials via High-Energy Mechanochemical Technique. *Prog. Mater. Sci.* 53 (2), 207–322. doi:10.1016/j.pmatsci.2007.05.001

Kothari, D., Raghavendra Reddy, V., Sathe, V. G., Gupta, A., Banerjee, A., and Awasthi, A. M. (2008). Raman Scattering Study of Polycrystalline Magnetoelectric $BiFeO_3$. *J. Magnetism Magn. Mater.* 320 (3-4), 548–552. doi:10.1016/j.jmmm.2007.07.016

Lagarec, K., and Rancourt, D. G. (1998). *Recoil-Mössbauer Spectral Analysis Software for Windows, Version 1.02*. Ottawa: Department of Physics, University of Ottawa.

Landers, J., Salamon, S., Escobar Castillo, M., Lupascu, D. C., and Wende, H. (2014). Mössbauer Study of Temperature-dependent Cycloidal Ordering in $BiFeO_3$ Nanoparticles. *Nano Lett.* 14 (11), 6061–6065. doi:10.1021/nl5031375

Li, W., Wang, F., Fu, G., Ren, Z., and Han, G. (2019). Ferroelectric Polarization Induced Selective Growth of $BiFeO_3$ Nanocrystals with a Remarkable Ferromagnetism. *Eur. J. Inorg. Chem.* 2019 (14), 1945–1950. doi:10.1002/ejic.201900053

Mao, W., Wang, X., Chu, L., Zhu, Y., Wang, Q., Zhang, J., et al. (2016). Simultaneous Enhancement of Magnetic and Ferroelectric Properties in Dy and Cr Co-doped $BiFeO_3$ Nanoparticles. *Phys. Chem. Chem. Phys.* 18 (9), 6399–6405. doi:10.1039/c5cp07327h

Mazumder, R., Sujatha Devi, P., Bhattacharya, D., Choudhury, P., Sen, A., and Raja, M. (2007). Ferromagnetism in Nanoscale $BiFeO_3$. *Appl. Phys. Lett.* 91 (6), 062510. doi:10.1063/1.2768201

Menil, F. (1985). Systematic Trends of the ^{57}Fe Mössbauer Isomer Shifts in (FeO_n) and (FeF_n) Polyhedra. Evidence of a New Correlation between the Isomer Shift and the Inductive Effect of the Competing Bond T-X (→ Fe) (Where X Is O or F and T Any Element with a Formal Positive Charge). *J. Phys. Chem. Sol.* 46 (7), 763–789. doi:10.1016/0022-3697(85)90001-0

Michalchuk, A. A. L., Boldyreva, E. V., Belenguer, A. M., Emmerling, F., and Boldyrev, V. V. (2021). Tribochemistry, Mechanical Alloying, Mechanochemistry: What Is in a Name? *Front. Chem.* 9, 685789. doi:10.3389/fchem.2021.685789

Momma, K., and Izumi, F. (2011). VESTA 3 for Three-Dimensional Visualization of Crystal, Volumetric and Morphology Data. *J. Appl. Cryst.* 44 (6), 1272–1276. doi:10.1107/S0021889811038970

Park, T.-J., Papaefthymiou, G. C., Viescas, A. J., Moodenbaugh, A. R., and Wong, S. S. (2007). Size-Dependent Magnetic Properties of Single-Crystalline Multiferroic $BiFeO_3$ Nanoparticles. *Nano Lett.* 7 (3), 766–772. doi:10.1021/nl063039w

Pinheiro, A. V. B., da Silva, R. B., Morales, M. A., Silva Filho, E. D., and Soares, J. M. (2020). Exchange Bias and Superspin Glass Behavior in Nanostructured $CoFe_2O_4$-Ag Composites. *J. Magnetism Magn. Mater.* 497, 165940. doi:10.1016/j.jmmm.2019.165940

Rodríguez-Carvajal, J. (2019). *FullProf Suite*. Grenoble: Institute Laue-Langevin.

Sánchez-De Jesús, F., Bolarín-Miró, A. M., Cortés-Escobedo, C. A., Barba-Pingarrón, A., and Pedro-García, F. (2020). Enhanced Ferromagnetic and Electric Properties of Multiferroic $BiFeO_3$ by Doping with Ca. *J. Alloys Comp.* 824, 153944. doi:10.1016/j.jallcom.2020.153944

Selbach, S. M., Tybell, T., Einarsrud, M.-A., and Grande, T. (2007). Size-Dependent Properties of Multiferroic $BiFeO_3$ Nanoparticles. *Chem. Mater.* 19 (26), 6478–6484. doi:10.1021/cm071827w

Šepelák, V., Becker, K. D., Bergmann, I., Suzuki, S., Indris, S., Feldhoff, A., et al. (2009). A One-step Mechanochemical Route to Core–Shell Ca_2SnO_4 Nanoparticles Followed by ^{119}Sn MAS NMR and ^{119}Sn Mössbauer Spectroscopy. *Chem. Mater.* 21 (12), 2518–2524. doi:10.1021/cm900590d

Šepelák, V., Bergmann, I., Feldhoff, A., Heitjans, P., Krumeich, F., Menzel, D., et al. (2007). Nanocrystalline Nickel Ferrite, $NiFe_2O_4$: Mechanosynthesis, Nonequilibrium Cation Distribution, Canted Spin Arrangement, and Magnetic Behavior. *J. Phys. Chem. C* 111 (13), 5026–5033. doi:10.1021/jp067620s

Šepelák, V., Düvel, A., Wilkening, M., Becker, K.-D., and Heitjans, P. (2013). Mechanochemical Reactions and Syntheses of Oxides. *Chem. Soc. Rev.* 42 (18), 7507–7520. doi:10.1039/c2cs35462d

Šepelák, V., Feldhoff, A., Heitjans, P., Krumeich, F., Menzel, D., Litterst, F. J., et al. (2006). Nonequilibrium Cation Distribution, Canted Spin Arrangement, and Enhanced Magnetization in Nanosized $MgFe_2O_4$ Prepared by a One-step Mechanochemical Route. *Chem. Mater.* 18 (13), 3057–3067. doi:10.1021/cm0514894

Sharma, V., Ghosh, R. K., and Kuanr, B. K. (2019). Investigation of Room Temperature Ferromagnetism in Transition Metal Doped $BiFeO_3$. *J. Phys. Condens. Matter* 31 (39), 395802. doi:10.1088/1361-648X/ab29d1

Ting, Y., Tu, C.-S., Chen, P.-Y., Chen, C.-S., Anthoniappen, J., Schmidt, V. H., et al. (2017). Magnetization, Phonon, and X-ray Edge Absorption in Barium-Doped $BiFeO_3$ Ceramics. *J. Mater. Sci.* 52 (1), 581–594. doi:10.1007/s10853-016-0355-0

Wang, T., Ma, Q., and Song, S.-H. (2018). Highly Enhanced Magnetic Properties of $BiFeO_3$ Nanopowders by Aliovalent Element Ba-Zr Co-doping. *J. Magnetism Magn. Mater.* 465, 375–380. doi:10.1016/j.jmmm.2018.06.034

Wang, X., and Wang, X. (2018). Room-temperature Magnetic Control of Ferroelectric Polarization and Enhanced Ferromagnetic Properties in $0.8BiFeO_3$-$BaTiO_3$ Ceramic. *Ceramics Int.* 44 (16), 19131–19134. doi:10.1016/j.ceramint.2018.06.131

Widatallah, H. M., Al-Qayoudhi, M. S., Gismelseed, A., Al-Rawas, A., Al-Harthi, S. H., Khalafalla, M. E. H., et al. (2014). Mechanosynthesis, Magnetic and Mössbauer Characterization of Pure and Ti^{4+}-Doped Cubic Phase $BiFeO_3$ Nanocrystalline Particles. *Hyperfine Interact* 226 (1-3), 143–151. doi:10.1007/s10751-013-0978-3

Xian, H., Tang, L., Mao, Z., Zhang, J., and Chen, X. (2019). Bounded Magnetic Polarons Induced Enhanced Magnetism in Ca-Doped $BiFeO_3$. *Solid State. Commun.* 287, 54–58. doi:10.1016/j.ssc.2018.09.009

Xing, W., Ma, Y., Ma, Z., Bai, Y., Chen, J., and Zhao, S. (2014). Improved Ferroelectric and Leakage Current Properties of Er-Doped $BiFeO_3$ Thin Films Derived from Structural Transformation. *Smart Mater. Struct.* 23 (8), 085030. doi:10.1088/0964-1726/23/8/085030

Yang, C.-H., Kan, D., Takeuchi, I., Nagarajan, V., and Seidel, J. (2012). Doping $BiFeO_3$: Approaches and Enhanced Functionality. *Phys. Chem. Chem. Phys.* 14 (46), 15953–15962. doi:10.1039/c2cp43082g

Yang, Y., Infante, I. C., Dkhil, B., and Bellaiche, L. (2015). Strain Effects on Multiferroic $BiFeO_3$ Films. *Comptes Rendus Physique* 16 (2), 193–203. doi:10.1016/j.crhy.2015.01.010

Yang, Y., Sun, J. Y., Zhu, K., Liu, Y. L., Chen, J., and Xing, X. R. (2009). Raman Study of $BiFeO_3$ with Different Excitation Wavelengths. *Physica B: Condensed Matter* 404 (1), 171–174. doi:10.1016/j.physb.2008.10.029

Zhong, J., Heremans, J. J., Viehland, D., Yee, G. T., and Priya, S. (2010). Ferromagnetism and Spin-glass-like Behavior of $BiFeO_3$ Nanoparticles. *Ferroelectrics* 400 (1), 3–7. doi:10.1080/00150193.2010.505521

Conflict of Interest: The authors declare that the research was conducted in the absence of any commercial or financial relationships that could be construed as a potential conflict of interest.

Publisher's Note: All claims expressed in this article are solely those of the authors and do not necessarily represent those of their affiliated organizations, or those of the publisher, the editors, and the reviewers. Any product that may be evaluated in this article, or claim that may be made by its manufacturer, is not guaranteed or endorsed by the publisher.